Bioorganic & Medicinal Chemistry 22 (2014) 2753–2762

Contents lists available at ScienceDirect

Bioorganic & Medicinal Chemistry

journal homepage: www.elsevier.com/locate/bmc

Synthesis and evaluation of a ^{18}F-curcumin derivate for β-amyloid plaque imaging

Johanna Rokka [a], Anniina Snellman [b], Cristiano Zona [c], Barbara La Ferla [c], Francesco Nicotra [c], Mario Salmona [d], Gianluigi Forloni [d], Merja Haaparanta-Solin [b], Juha O. Rinne [e], Olof Solin [a,f,*]

[a] Turku PET Centre, Radiopharmaceutical Chemistry Laboratory, University of Turku, Porthaninkatu 3, FI-20500 Turku, Finland
[b] Turku PET Centre, Preclinical Imaging, University of Turku, Tykistökatu 6, FI-20520 Turku, Finland
[c] Department of Biotechnology and Bioscience, University of Milano-Bicocca, I-20126 Milano, Italy
[d] Department of Biochemistry and Molecular Pharmacology, Istituto di Ricerche Farmacologiche 'Mario Negri', I-20156 Milano, Italy
[e] Turku PET Centre c/o Turku University Hospital, University of Turku, PO Box 52, FI-20521 Turku, Finland
[f] Turku PET Centre, Accelerator Laboratory, Åbo Akademi University, Porthansgatan 3, FI-20500 Turku, Finland

ARTICLE INFO

Article history:
Received 20 December 2013
Revised 4 March 2014
Accepted 10 March 2014
Available online 18 March 2014

Keywords:
Positron emission tomography (PET)
Nucleophilic ^{18}F-fluorination
Curcumin
Alzheimer's disease
Click chemistry
β-Amyloid

ABSTRACT

Introduction: Curcumin is a neuroprotective compound that inhibits the formation of amyloid oligomers and fibrils and binds to β-amyloid plaques in Alzheimer's disease (AD). We aimed to synthesize an ^{18}F-labeled curcumin derivate ([^{18}F]**4**) and to characterize its positron emission tomography (PET) tracer-binding properties to β-amyloid plaques in a transgenic APP23 mouse model of AD.
Methods: We utilized facile one-pot synthesis of [^{18}F]**4** using nucleophilic ^{18}F-fluorination and click chemistry. Binding of [^{18}F]**4** to β-amyloid plaques in the transgenic APP23 mouse brain cryosections was studied in vitro using heterologous competitive binding against PIB. [^{18}F]**4** uptake was studied ex vivo in rodents and in vivo using PET/computed tomography of transgenic APP23 and wild-type control mice.
Results: The radiochemical yield of [^{18}F]**4** was 21 ± 11%, the specific activity exceeded 1 TBq/μmol, and the radiochemical purity exceeded 99.3% at the end of synthesis. In vitro studies of [^{18}F]**4** with the transgenic APP23 mouse revealed high β-amyloid plaque binding. In vivo and ex vivo studies demonstrated that [^{18}F]**4** has fast clearance from the blood, moderate metabolism but low blood–brain barrier (BBB) penetration.
Conclusions: [^{18}F]**4** was synthesized in high yield and excellent quality. In vitro studies, metabolite profile, and fast clearance from the blood indicated a promising tracer for Aβ imaging. However, [^{18}F]**4** has low in vivo BBB penetration and thus further studies are needed to reveal the reason for this and to possibly overcome this issue.

1. Introduction

Curcumin (also known by its chemical formula, 1,6-heptadiene-3,5-dione-1,7bis(4-hydroxy-3-methoxyphenyl)-(1*E*,6*E*) or 1,1-diferuloylmethane) is the active ingredient in the Indian spice turmeric (*Curcuma longa*) and is known to be responsible for the medicinal effects of turmeric.[1,2] Curcumin is a neuroprotective compound that inhibits the formation of amyloid oligomers and fibrils and binds to β-amyloid (Aβ) plaques found in Alzheimer's disease (AD) with high binding potential.[3,4] Curcumin has also been shown to reduce Aβ deposits in the brains of Tg2576 mice in vivo.[3,5] Although curcumin is not toxic (even in large doses), it has poor physiological properties. In vivo clinical studies show fast metabolism and poor absorption of curcumin.[1,2,4,6] Therefore, there has been considerable recent interest in developing curcumin analogues as drug candidates and imaging tracers.[7–15]

Curcumin has a tautomeric structure with two carbonyl groups that can interconvert to keto–enol forms (Fig. 1). Studies that employ curcumin derivates demonstrate that the enol form predominates when curcumin and its derivates are bound to Aβ aggregates.[16–18] Structure–activity relationship studies have shown that the Aβ plaque-binding properties of curcumin are due to its planar structure, which consists of two terminal phenyl groups with proper substituents and an appropriate linker length with double bond conjugation and narrow flexibility.[18,19] Also

* Corresponding author. Fax: +358 2 231 8191.
E-mail address: olof.solin@utu.fi (O. Solin).

http://dx.doi.org/10.1016/j.bmc.2014.03.010
0968-0896/

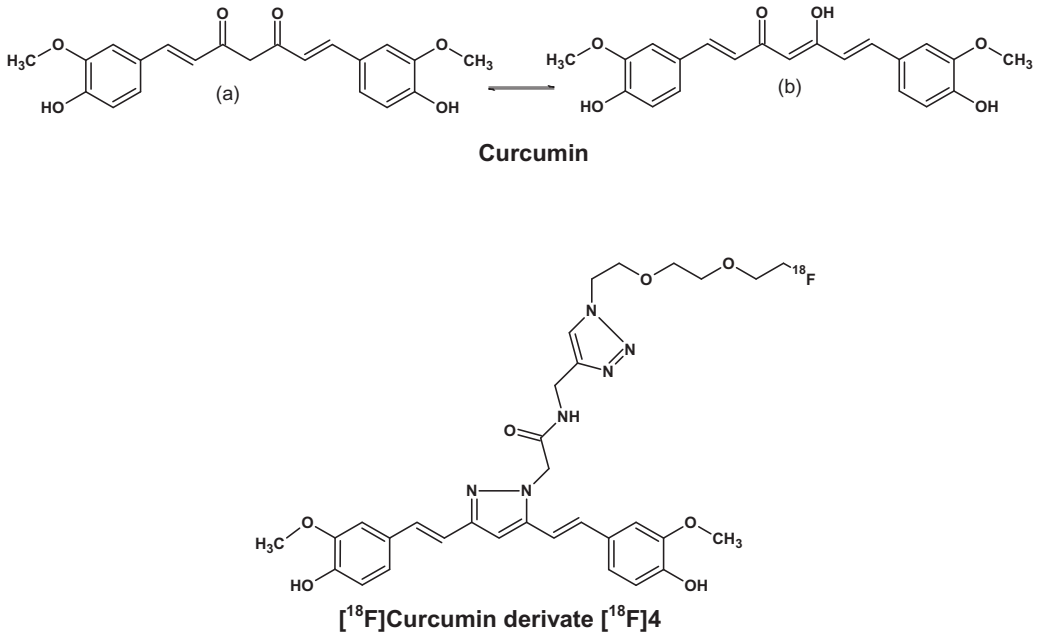

Figure 1. Chemical structures of curcumin, the [^{18}F]curcumin derivate ([^{18}F]**4**. Curcumin exists in equilibrium between keto (a) and enol (b) forms.

the delocalization of charge through the structure facilitates deprotonation of the phenolic group, which improves the Aβ binding of curcumin.[18]

Because of their Aβ plaque-binding properties, curcumin derivates labeled with positron-emitting radionuclides are potential tracers for positron emission tomography (PET) imaging in AD.[7,8,10,12,14] PET is a noninvasive imaging method that can be used to visualize Aβ plaques in patients with mild cognitive impairment or AD.[20] The ^{11}C-labelled thioflavin derivate [^{11}C]2-(4′-(methylamino)phenyl)-6-hydroxybenzothiazole ([^{11}C]PIB) is an extensively studied and used PET tracer because of its highly specific Aβ plaque-binding ability.[21,22] Numerous new PET tracers for Aβ imaging in AD are currently under development.[23–28] This research focuses on thioflavin and stilbene derivates.[25–28] The potential of radiolabelled curcumin derivates is often ignored,[23,24] although several studies have shown strong binding of curcumin derivates to Aβ, and even capability to reduce Aβ burden.[1–5,7,9,11–18]

The purpose of this study was to synthesize a ^{18}F-labeled curcumin derivate [^{18}F]**4** (Fig. 1) and to characterize its tracer binding properties to Aβ plaques. We describe a facile one-pot synthesis of [^{18}F]**4** using nucleophilic ^{18}F-fluorination and click chemistry (Fig. 2), and show that [^{18}F]**4** binds specifically to Aβ plaques in post-mortem brain sections of transgenic APP23 mice. Although in vitro autoradiography studies, calculated partition coefficient, metabolite profile, and fast clearance from the blood indicated a promising tracer for Aβ imaging, in vivo studies with [^{18}F]**4** showed little penetration of the blood–brain barrier (BBB).

2. Materials & methods

2.1. Precursors and reference compounds

The nonradioactive compounds 2-[2-(2-azidoethoxy)ethoxy] ethyl tosylate (**1**), 2-[2-(2-azidoethoxy)ethoxy]ethylfluoride (**2**), 2-[3,5-bis(4-hydroxy-3-methoxystyryl)-1*H*-pyrazol-1-yl]-*N*-(prop-2-yn-1-yl) acetamide (**3**), and 2-[3,5-bis(4-hydroxy-3-methoxystyryl)-1*H*-pyrazol-1-yl]-*N*-{1-[2-(2-(2-fluoroethoxy)ethoxy)ethyl)-1*H*-1,2,3-triazol-4-yl]methyl}acetamide (**4**) were synthesized at the Department of Biotechnology and Biosciences, University of Milano-Bicocca (see Supplementary data).

2.2. Materials for labelling synthesis

Organic solvents were high performance liquid chromatography (HPLC) grade from Rathburn Chemicals Ltd (Walkernburn, Great Britannia). Water was purified using a Milli-Q Plus Ultra Pure Water system (Millipore, Molsheim, France). Other chemicals were analytical grade from Merck (Darmstadt, Germany). Thin layer chromatography (TLC) plates were glass plates pre-coated with high performanceTLC (HPTLC) Silica gel 60 RP-18 F_{254}s (art. no 113724) and aluminum plates pre-coated with Silica 60 F_{254}s (art. no 1.05554) from Merck (Darmstadt, Germany).

2.3. Radiosynthesis procedure

2.3.1. ^{18}F-fluoride production

^{18}F-fluoride was produced using the ^{18}O(p,n)^{18}F nuclear reaction. ^{18}O-enriched water (enrichment grade 98%, volume 800 μl, Hyox, Rotem Industries Ltd, Israel) was irradiated with 17 MeV protons of 10 μA beam current for 15 min using the MGC-20 cyclotron (Efremov Scientific Research Institute for Electrophysical Apparatuses (NIIEFA), St. Petersburg, Russia). The activity of ^{18}F was approximately 7 GBq at the start of synthesis.

2.3.2. General procedure for nucleophilic ^{18}F-fluorine labeling reaction

The aqueous solution of ^{18}F-fluoride from the cyclotron target chamber was collected into a borosilicate glass reaction vessel containing 4.7 mg (3.9–5.6 mg) potassium carbonate and 16.8 mg (15.2–18.3 mg) Kryptofix 222. Water was removed using an azeotropic distillation procedure, during which 1 ml acetonitrile was added to the solution. The solution was then heated to 100 °C for 3 min and evaporated using reduced pressure and a stream of helium gas. This process was repeated three times. 1.1 mg (0.7–1.3 mg) of precursor **1** was dissolved in 500 μl DMSO and added to the dry ^{18}F-fluoride–Kryptofix complex. The reaction mixture was heated at 100 °C for 2 min and then cooled at room temperature for 3 min. A sample was taken from the reaction mixture for analysis. Subsequently, 1.8 mg (1.7–2.0 mg) of compound **3** was dissolved in 250 μl of DMSO, and this solution was added to the reaction vessel. A freshly made

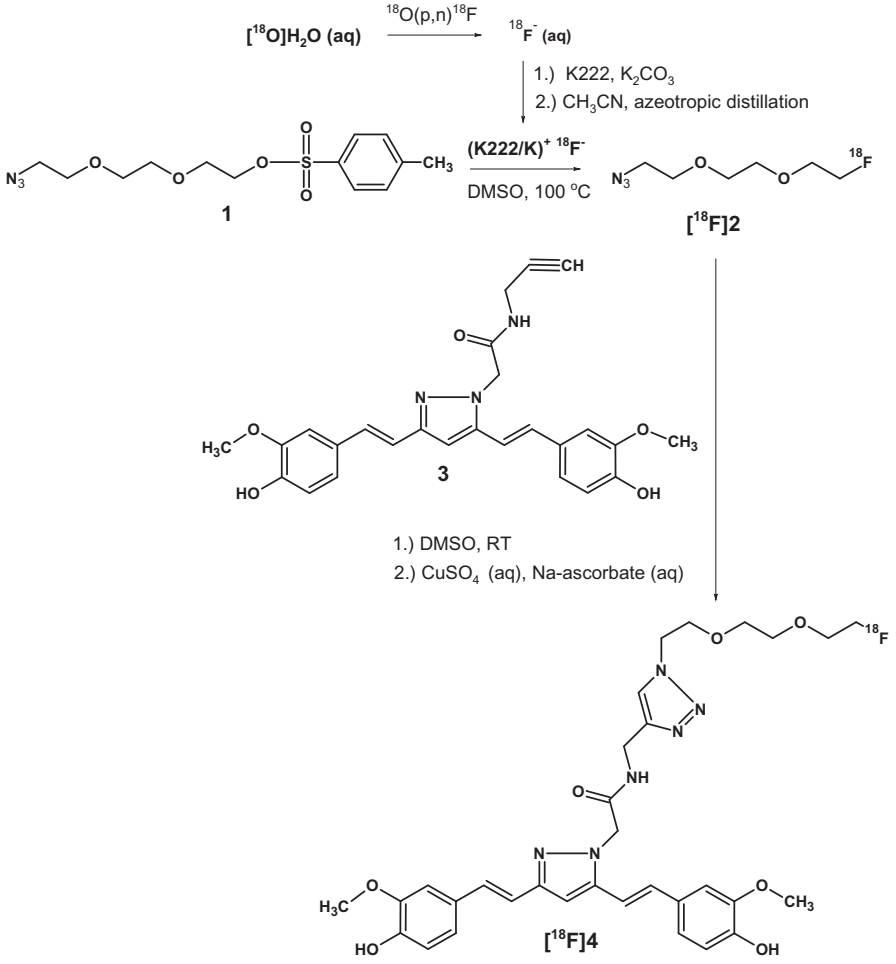

Figure 2. Reactions and reaction conditions of [^{18}F]**4** radiosynthesis. Nucleophilic ^{18}F-fluorination using ^{18}F-fluoride–Kryptofix complex was employed to produce [^{18}F]**2**. Without intermediate purification, [^{18}F]**2** was clicked with **3** to produce [^{18}F]**4**.

aqueous catalyst mixture containing 5 μmol of $CuSO_4{\cdot}5\ H_2O$ and 6 μmol of sodium ascorbate was added to the reaction vessel. The reaction proceeded for 15 min at room temperature. Before semi-preparative HPLC purification, 1 ml water was added to the vessel.

The product [^{18}F]**4** was separated from the reaction mixture using semi-preparative HPLC. A Merck Hitachi LaChrom 7000 pump (Merck Hitachi, Darmstadt, Germany) was used together with a Phenomenex Luna 5u C18(2) 100A (250 × 10.0 mm) column (Phenomenex, Allerød, Denmark). UV absorption and radioactivity were monitored at the outflow of the column using a Merck Hitachi LaChrom UV detector and a NaI(Tl) scintillation detector (2 × 2 inches, Bicron Corporation, Newbury, OH, USA) connected in series.

The mobile phase was a gradient of 1% acetic acid containing 200 mg/l ascorbic acid (**A**) or methanol (**B**). The gradient profile was 0–3 min of 100% **A**, 3.1 min of 60% **A**: 40% **B**, 40 min of 10% **A**: 90% **B**, with a flow rate of 5.0 ml/min. The collected fraction of [^{18}F]**4** was subsequently purified using solid phase extraction (Sep-Pak® light tC18 cartridge, Waters). During this procedure, the HPLC fraction was first diluted with 20 ml buffer A which contained 200 mg/l ascorbic acid in 0.1 M phosphate buffer (pH 7.4). This solution was passed through a Sep-Pak cartridge. Next, the cartridge was washed with 20 ml of buffer A. Finally [^{18}F]**4** was eluted from the cartridge using 0.4 ml ethanol, and the fraction was diluted with 4.0 ml of buffer A.

2.4. Analytical procedures

After radiofluorination, the radiochemical yield of [^{18}F]**2** was determined with silica 60 F_{254}s thin layer plates developed with a mixture of petrol ether/ethyl acetate (1:1 v/v). The progression of the click reaction was followed by analyzing samples from the reaction with HPTLC plate Silica gel 60 RP-18 F_{254}s developed using a mixture of 1% acetic acid: methanol (2:8 v/v). The amount of radioactive compound on the plate was analyzed using photostimulated luminescence (PSL) autoradiography. The developed TLC plate was placed into an exposure cassette with an imaging plate (Fuji Imaging Plate BAS-MS2025, Fuji Photo Film Co., Ltd, Tokyo, Japan). After exposure, the imaging plate was scanned using a Fuji Analyser BAS 1800 reader (Fujifilm Co., Ltd, Tokyo, Japan) at 200 μm resolution. Data were analyzed using the Tina 2.1 program (Raytest Isotopenmessgeräte GmbH, Straubenhardt, Germany).

The specific radioactivity, radiochemical purity, and chemical purity of [^{18}F]**4** were analyzed using an analytical HPLC method and a Merck Hitachi LaChrom 7000 system with Hitachi D-7000 HPLC System Manager (HSM) software (version 3.0). The wavelength of the UV detector was set at 330 nm and the radioactivity was measured with a similar NaI(Tl) scintillation detector as described above. Analysis was conducted using a Phenomenex Gemini-NX 3u C18 110A (150 × 4.60 mm) column and an isocratic system with an eluent of 1% acetic acid/methanol (51:49 v/v) and a flow rate of 0.8 ml/min. The concentration of **4** was analyzed using

linear calibration with an authentic standard of known concentrations. The corresponding peak observed at the radioactivity detector was collected and the radioactivity of this HPLC fraction was analyzed. Using this method, the radiochemical purity was also measured for up to 6 h to ensure the stability of the end product [^{18}F]**4** dissolved in the formulation solution (ethanol–buffer A, 1:10 v/v).

2.5. *C*log*P* calculations

The partition coefficients (*C*log*P*) of curcumin, [^{18}F]**4**, and PIB were calculated using the Molinspiration property engine software, v2011.04 (http://www.molinspiration.com/).

2.6. Animal studies

Animal studies were performed with Sprague Dawley rat, C57Bl/6N mouse (bred in the animal facility of the University of Turku), and transgenic APP23[29] mice and corresponding wild-type (WT) control mice (Novartis Pharma, Switzerland). Animal experiments were approved by the Animal Experiment Board of the Province of Southern Finland.

2.6.1. In vitro binding studies

The binding of [^{18}F]**4** to Aβ plaques was studied using 20-μm, post-mortem brain cryosections from a transgenic APP23 mouse at the age of 18 months and from a WT mouse at the age of 28 months. The mice were sacrificed via cardiac puncture in deep isoflurane anesthesia. The brains were immediately removed and frozen by immersion in isopentane chilled with dry ice. Twenty-micrometer brain sections were cut using a cryomicrotome (Leica Microsystems Nussloch GmbH, Nussloch, Germany) and thaw-mounted onto glass slides. Sections on glass slides were stored at −20 °C until use.

The binding of [^{18}F]**4** to Aβ plaques in the cryosections was studied using heterologous competitive binding against PIB (K_i = 4.3 nM for Aβ plaques [21]). Cryosections were thawed to room temperature 15 min before use and were not pretreated. Sections were preincubated in 4% human serum albumin in phosphate buffer solution (HSA-solution) for 10 min, followed by 30 min incubation in 0.5 MBq/ml of [^{18}F]**4** in HSA-solution. For competitive binding studies, various concentrations (0–400 μM) of PIB (ABX GmbH, Radeberg, Germany) were added to the incubation solution. Adjacent sections from the mouse brains were used. After incubation, sections were washed twice for 5 min in the HSA-solution and with two additional 5-min washes in phosphate buffer solution. Finally, sections were briefly rinsed with water and rapidly dried in a stream of air.

The brain sections were then apposed to an imaging plate for 3 h. The plates were scanned with a Fuji FLA-5100 laser scanner (Fuji Photo Film Co., Tokyo, Japan) using 10-μm resolution. The digital autoradiography images were analyzed using AIDA image analysis software, version 4.06 (Raytest Isotopenmessgeräte GmbH, Straubenhardt, Germany).

The presence and localization of Aβ plaques were confirmed with Thioflavin S staining of the same brain sections that were used for the [^{18}F]**4** binding studies.

Specific uptake of [^{18}F]**4** was calculated as PSL per area and was determined from cortical section areas with high plaque load, as observed with Thioflavin S staining, a routine histological staining for Aβ plaques. Non-specific uptake was determined in a similar manner from caudate/putamen areas where no Thioflavin S staining was observed. A competitive binding curve was constructed from the data using a sigmoid fit. From this curve, the half maximal inhibitory concentration (IC_{50}) was determined.

2.6.2. In vivo studies

In vivo biodistribution of [^{18}F]**4** was evaluated in two transgenic female APP23 mice[29] at the age of 16 months (animal weights 22.0 g and 23.0 g) and in two female WT mice at the age of 25 months (animal weights 31.9 g and 25.8 g). In vivo PET was performed with the Inveon Multimodality PET/computed tomography (CT) device (Siemens Medical Solutions, Knoxville, TN, USA). Animals were anesthetized using 2.5% isoflurane/O_2, and CT was conducted for attenuation correction and anatomical reference. Subsequently, 3.8 ± 1.2 MBq [^{18}F]**4** was injected into the tail vein and dynamic 60-min PET scans were initiated. Data were collected in 3D list mode, divided into 51 time frames (30 × 10; 15 × 60; 4 × 300; 2 × 600 s), and reconstructed using the 2D filtered back-projection algorithm. Dynamic data were analyzed using the Inveon Research Workplace analysis tool v. 4 (Siemens Medical Solutions). Regions of interest (ROIs) were drawn to whole brain, frontal cortex, cerebellum, liver, kidney, intestine, heart, and vena cava for the estimation of radioactivity in the blood. ROIs were defined to co-registered CT images used as anatomical reference, and further guided by mouse brain atlas for frontal cortex and cerebellum, or radioactivity uptake for the peripheral organs of interest. Subsequently ROIs were transformed to the PET image to obtain the time-radioactivity curves and results were presented as percentages of the injected dose per gram of tissue (%ID/g). Specific [^{18}F]**4** binding to Aβ plaques in APP23 brain was estimated from frontal cortex-to-cerebellum ratios.

2.6.3. Ex vivo studies

Distribution of [^{18}F]**4** in the brain ex vivo was evaluated in one male C57Bl/6N mouse (animal weight 28.0 g, injected dose 9.8 MBq) and one male Sprague Dawley rat (animal weight 271 g, injected dose 34.4 MBq). The tracer was allowed to distribute for 10 min. The animals were sacrificed via cardiac puncture in deep isoflurane anesthesia. Cardiac blood samples were collected in gel-lithium heparin tubes (Terumo Europe N.V., Leuven, Belgium); the brains were rapidly dissected, weighed, and radioactivity was measured using a NaI(Tl) well counter (3″ × 3″, Bicron, Newbury, OH, USA). Subsequently, the brains were frozen in chilled isopentane on dry ice, cut into 20-μm cryosections using a cryomicrotome (Leica Microsystems Nussloch GmbH), air dried, and exposed to an imaging plate (Fuji Imaging Plate BAS-TR2025, Fuji Photo Film Co.) for approximately four hours. The plates were scanned with a Fuji BAS 5000 Analyzer using 25-μm resolution.

The amounts of unchanged [^{18}F]**4** and its radioactive metabolites were analyzed from rat plasma at 10 min post [^{18}F]**4** injection. Plasma and erythrocytes were separated by centrifugation (1300*g*, 10 min), and proteins were precipitated from the sample with methanol. After centrifugation, 10 μl of the supernatant were applied to a HPTLC Silica gel 60 RP-18W plate (Merck, art. no 1.14296, Darmstadt, Germany) together with a [^{18}F]**4** standard sample from the used synthesis batch. The plate was developed, exposed, and scanned as previously described for the progression of the click reaction. The images were analyzed using AIDA Image Analyzer v.4.19 (Raytest Isotopenmessgeräte GmbH).

2.7. Statistics

Mean values were calculated from the individual measurements and expressed at a precision of one standard deviation (mean ± SD). Saturation binding analyses were performed with GraphPad Prism, version 2.01 (GraphPad Software, San Diego, CA, USA).

3. Results

3.1. Radiosynthesis of [^{18}F]4

The ^{18}F-curcumin derivate [^{18}F]**4** was synthesized using a one-pot synthesis procedure (Fig 2). After radiofluorination, the radiochemical yield of [^{18}F]**2** was 77 ± 10%, decay corrected to the end of cyclotron bombardment (n = 9, Fig. 3A and Supplementary data Fig. 1A). Without intermediate purification, [^{18}F]**2** and **3** were clicked together using in situ prepared Cu(I) as the catalyst for the reaction (Fig. 3B and Supplementary data Fig. 1B). The end product [^{18}F]**4** was purified using semipreparative HPLC. The non-optimized radiochemical yield of [^{18}F]**4** was 21 ± 11% at the end of synthesis (EOS) (n = 9, Supplementary data Fig. 1C), and the specific radioactivity exceeded 1 TBq/μmol at the EOS. The radiochemical purity of [^{18}F]**4** was 99.3% (96.5–100%, SD 1.2%). The radiochemical purity of the final product remained unchanged over the course of 6 h after synthesis.

3.2. *C*Log*P*

The *C*log*Ps* for curcumin, [^{18}F]**4**, and PIB were 2.3, 3.0, and 3.6, respectively.

3.3. Animal studies

3.3.1. In vitro binding of [^{18}F]4

To evaluate the binding of [^{18}F]**4** to fibrillar Aβ, in vitro autoradiography was performed using *post mortem* brain cryosections (n = 17) from an APP23 and a WT mouse. PSL autoradiography images of stained APP23 brain sections revealed [^{18}F]**4** binding to fibrillar Aβ deposits located in cortical areas. The presence of fibrillar Aβ plaques was verified by staining the same sections with Thioflavin S (Fig. 4). In brain sections from the WT mouse, Thioflavin S staining detected no plaques and the autoradiographs detected only non-specific binding of the tracer (Fig. 4).

In a separate experiment specific [^{18}F]**4** uptake was displaced by incubating APP23 mouse brain tissue slices (n = 4) with various concentrations of PIB. Nonspecific binding of [^{18}F]**4** was defined as binding at the caudate/putamen brain area of the same section, where no Aβ plaques were found. Figure 5 shows Aβ binding of [^{18}F]**4** as a function of increasing PIB concentration. The IC_{50} value for this displacement was 10^{-4} M.

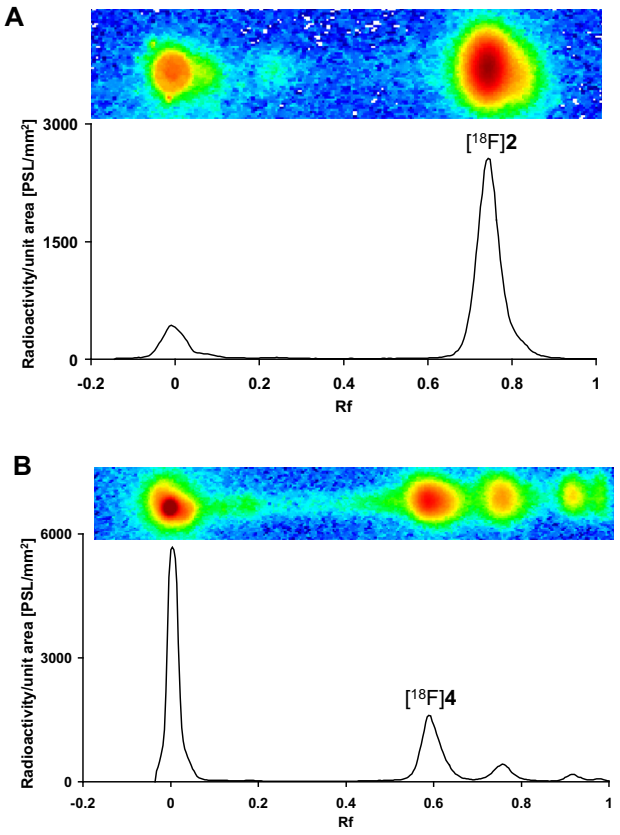

Figure 3. TLC analysis of reaction mixture after ^{18}F-radiofluorination (A) using silica 60 F_{254}s thin layer plates with a mixture of petrol ether/ethyl acetate (1:1, v/v). TLC analysis of the reaction mixture after the click reaction (B) using HPTLC Silica gel 60 RP-18 F_{254}s thin layer plates with a mixture of 1% acetic acid: methanol (2:8, v/v) and autoradiography.

3.3.2. Biodistibution of [^{18}F]4

The in vivo biodistribution of [^{18}F]**4** in a representative WT mouse during a 60-min dynamic PET scan is presented in Figure 6A. Rapid clearance of ^{18}F-radioactivity from blood and immediate uptake into the liver was seen in the initial phase of the scan. At a later phase, high and persistent uptake occurred in the intestine (Fig. 6A). ^{18}F-radioactivity uptake to the brains of representative transgenic APP23 and WT mice is presented in Figure 6B. Immediately after injection (0–1 min), ^{18}F-radioactivity in the blood was high, and the blood circulation in the brain was visible. However, as ^{18}F-radioactivity in the blood decreased (1–5 min), very low ^{18}F-radioactivity was detected in the brains of APP23 and WT mice. Increased retention of [^{18}F]**4** was not detected in the APP23 brain, which harbored abundant Aβ deposition in comparison to the WT brain, which lacked binding sites for [^{18}F]**4**. No increase in frontal cortex-to-cerebellum ratios were seen in APP23 brain. The ratios calculated for the last imaging frame (40–60 min p.i.,) were 1.00 and 0.98 for APP23 TG mice, and 0.82 and 0.96 for WT mice. Time-radioactivity curves for blood and brain for APP23 and WT mice are presented in Figure 6B.

3.3.3. Ex vivo studies

Entrance of [^{18}F]**4** to the brain was further investigated using ex vivo digital autoradiography and tissue counting of C57Bl/6N mouse and Sprague Dawley rat brains at 10 min post [^{18}F]**4** injection. ^{18}F-radioactivity in the whole brain was low in the mouse (0.04% ID/g) and rat brains (0.03% ID/g); digital autoradiography indicated that the highest ^{18}F-radioactivity occurred in the brain ventricles (Fig. 7A, B).

3.3.4. Metabolism of [^{18}F]4

The parent compound [^{18}F]**4** (R_f = 0.6) and two polar radioactive metabolites, M1 (R_f = 0.8) and M2 (R_f = 0.85), were detected in rat plasma 10 min after [^{18}F]**4** injection (Fig. 8). At 10 min after tracer injection, 45% of the total ^{18}F-radioactivity in the plasma was unchanged [^{18}F]**4**. M1 and M2 comprised 17% and 38% of the total ^{18}F-radioactivity, respectively. These metabolites were not characterized further.

4. Discussion

In this study we describe a one-pot synthesis of the ^{18}F-curcumin derivate [^{18}F]**4**. Initial radiofluorination of the labeling precursor [^{18}F]**2** was conducted using nucleophilic ^{18}F-fluorination. The reaction was efficient: the reaction mixture was heated for only 2 min at 100 °C to obtain a high yield of [^{18}F]**2**. Extending the reaction time did not improve the yield; on the contrary, it caused [^{18}F]**2** to degrade.

Click-reaction components were added to the reaction vessel without intermediate purification of [^{18}F]**2**. The reaction vessel

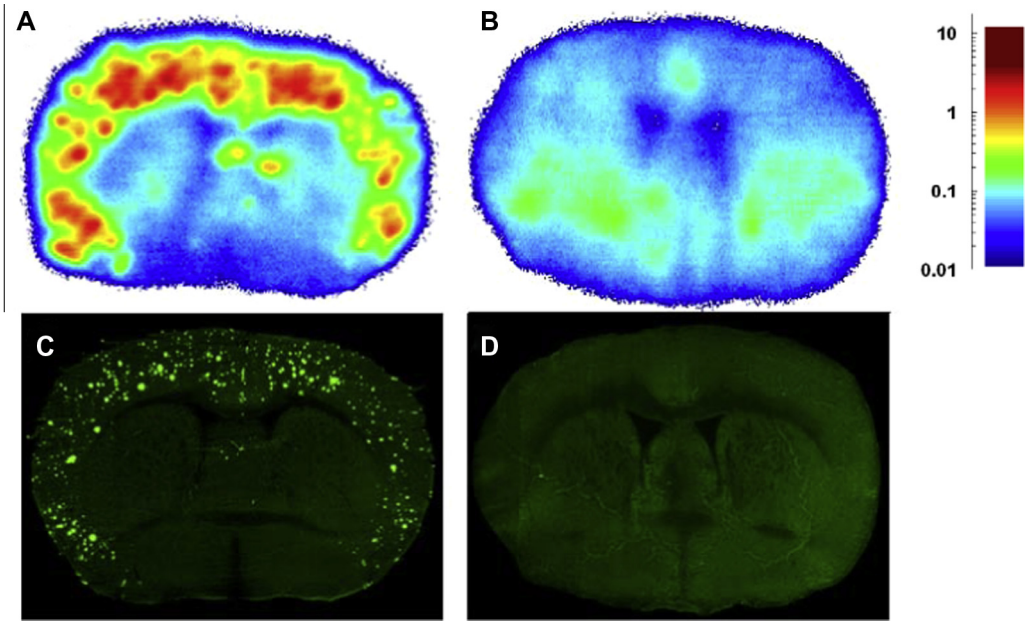

Figure 4. Representative in vitro autoradiographic images of brain sections from an APP23 mouse (A) and a WT mouse (B). The color bar on the right indicates the relative uptake of radioactivity. Images of the same brain sections after Thioflavin S staining (C, D). Thioflavin S staining appears as bright green.

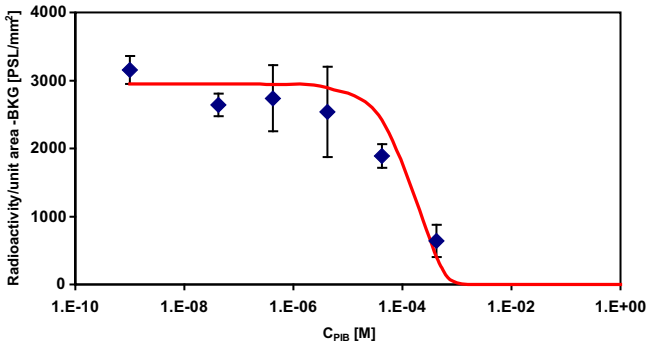

Figure 5. Competition binding curve fitted to displacement data. An IC_{50} of 10^{-4} M was determined for [^{18}F]**4** versus PIB.

was cooled to room temperature before addition of the other reaction components, as heat can cause decomposition of compounds **3** and [^{18}F]**4**. For the same reason, the click-reaction was performed at room temperature. The click-reaction catalyst, Cu(I), was prepared in situ through the reaction of copper sulfate with sodium ascorbate. A water solution of copper sulfate and sodium ascorbate was mixed and added to the click-reaction solution. This small amount of water was well tolerated by the click-reaction.

As previous studies [1,4,30] have shown, the low stability of curcumin and its derivates is a shortcoming for these compounds. [^{18}F]**4** has a structure that has been shown to improve the water solubility and chemical stability of the compound.[31] We further stabilized [^{18}F]**4** during the production process by carefully choosing the purification conditions, formulation procedure, and formulation solution. Curcumin and its derivates are usually more stabile in acidic than in neutral or basic aqueous solutions [30] and acidic conditions were favored in the purification procedure. During the synthesis development we noticed that the key element for stabilizing this curcumin derivate was the combination of alcohol and ascorbic acid. These additives drastically decreased the oxidative decomposition and radiolysis of [^{18}F]**4**. Therefore ascorbic acid was added in each solution used for purification and formulation of [^{18}F]**4**, methanol was the organic component of the preparative HPLC solvent and formulation solution contained ethanol. As a result, produced [^{18}F]**4** had high radiochemical purity that did not change at least over the course of 6 h after end of synthesis.

The *C*log*P* values of curcumin, [^{18}F]**4**, and PIB were calculated to estimate the lipophilicity of [^{18}F]**4**. These calculations showed that [^{18}F]**4** is expected to be more lipophilic than curcumin, but less lipophilic than PIB. Values from the calculations are estimates; however, they do provide an indication of the relative lipophilicities of these compounds. The measured log*P* value for PIB is 1.2.[21] For ^{18}F-labelled curcumin derivates measured log*P* values have varied from 1.8 to 3.7.[7,12,14] The *C*log*P* for [^{18}F]**4** is in line with the earlier measured values for ^{18}F-curcumin derivates and in the range that is usually considered close to optimal for in vivo BBB penetration for small molecules.[23,32,33]

Curcumin has been shown to bind to aggregated Aβ oligomers and fibrils, i.e. not to monomeric structures.[3–5] In vitro binding studies of [^{18}F]**4** with brain cryosections from APP23 and WT mice were used to evaluate tracer affinity to amyloidal plaques. Tissues were not treated beforehand because pretreatment might change nonspecific [^{18}F]**4** binding in white matter areas of the brain sections. The high log*P* value presumed high [^{18}F]**4** uptake in fatty tissue. Therefore, the low non-specific uptake of [^{18}F]**4** in fatty brain tissue in vitro is surprising. This property is of value for PET-tracers, as high non-specific uptake easily confounds interpretation of clinical PET images and data.

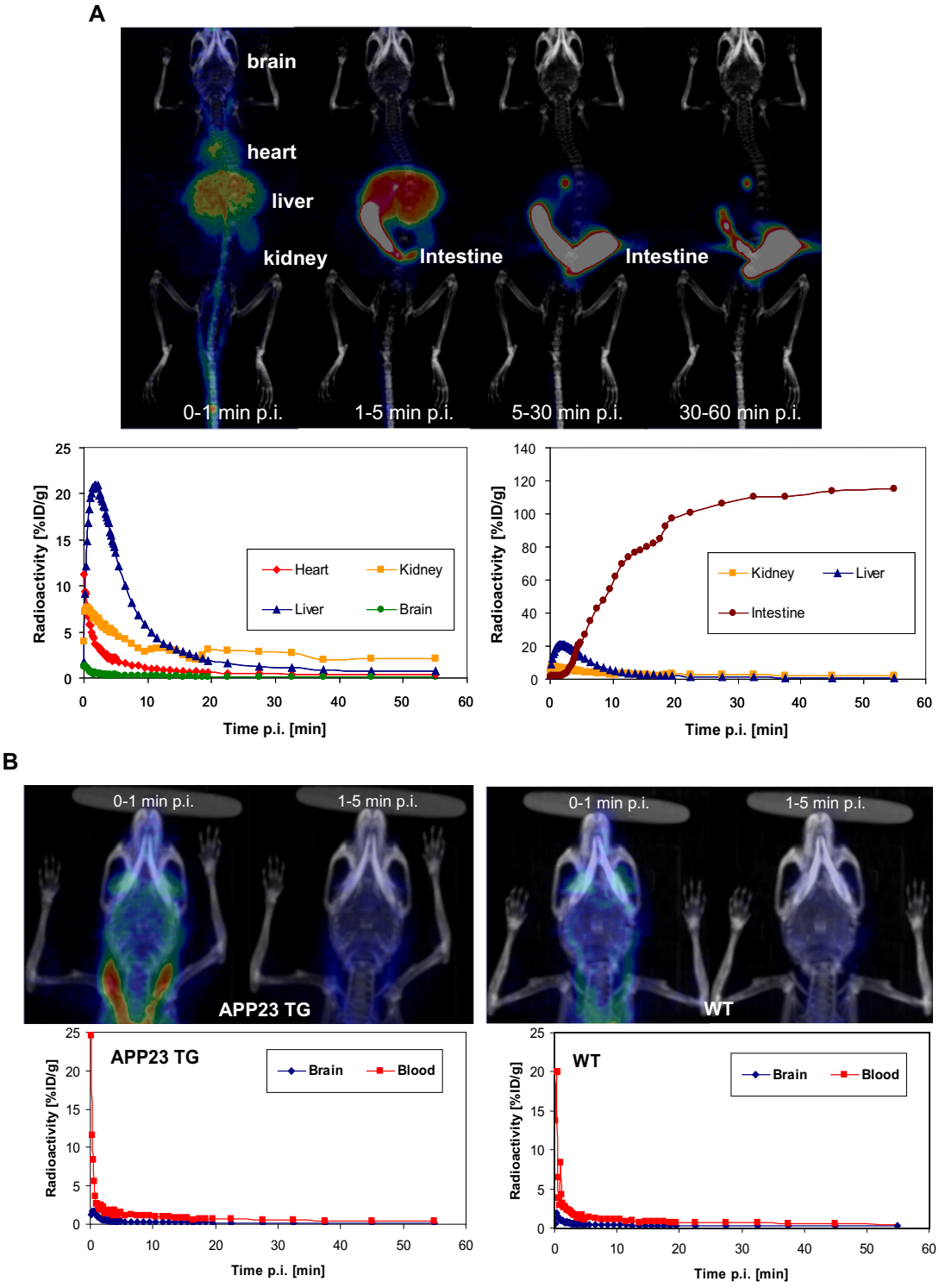

Figure 6. In vivo biodistribution and elimination of [^{18}F]**4** in a WT and APP23 mice. (A) In vivo biodistribution of [^{18}F]**4** in a representative WT mouse (25 months old, injected dose 2.6 MBq, anesthetized using 2.5% isoflurane/O_2) and time-radioactivity curves for 0–60 min post injection (p.i.) for regions of interest. (B) Uptake of [^{18}F]**4** in the brain of a representative transgenic APP23 mouse (15 months old, injected dose 5.2 MBq, anesthetized using 2.5% isoflurane/O_2) and a representative WT mouse (25 months old, injected dose 4.4 MBq, anesthetized using 2.5% isoflurane/O_2), and time-radioactivity curves for blood and whole brain of the same mice.

[^{18}F]**4** binding was high in cortical areas of transgenic mouse brain and histochemical staining indicated that the Aβ plaque patterns were compatible with [^{18}F]**4** binding. These findings suggest that [^{18}F]**4** binds to Aβ plaques. In the transgenic mouse brain sections, cortical binding of [^{18}F]**4** was displaced by adding nonradioactive PIB to the incubation solution. PIB has high Aβ binding affinity (K_i 4.3 nM,[21]), and is therefore a proper displacement substance. Displacement with PIB did not change white matter binding in either the transgenic or the WT mouse. The combination of effective PIB displacement in the cortical areas of transgenic mouse brain and matching histochemical staining further confirms that [^{18}F]**4** binds mainly to Aβ plaques.

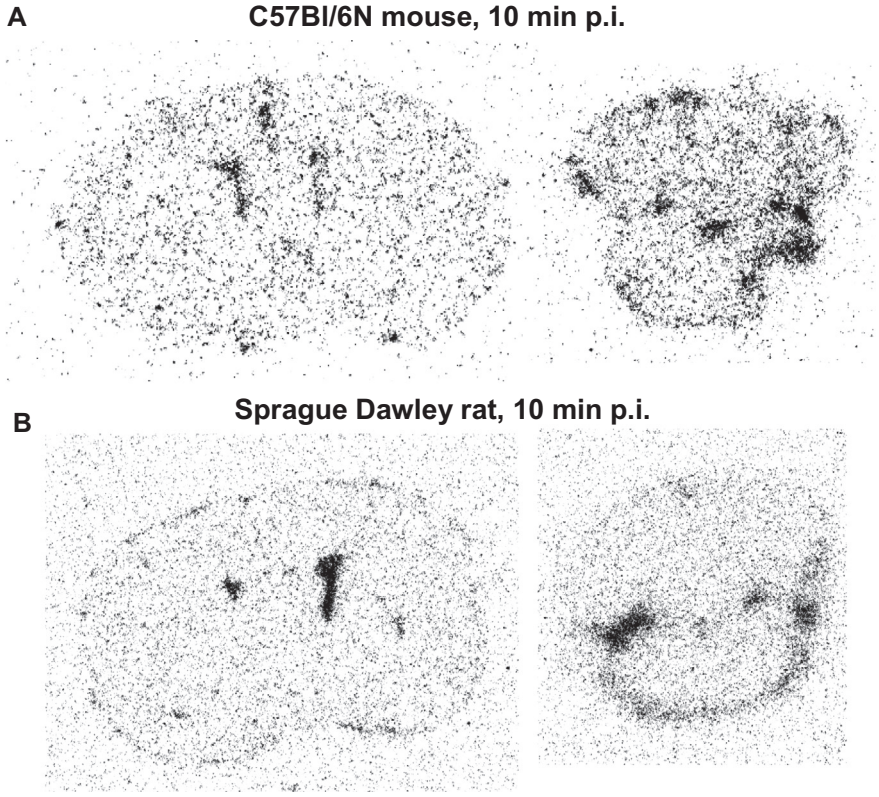

Figure 7. Ex vivo autoradiographic images of coronal ex vivo brain cryosections from a C57Bl/6N mouse (A) and a Sprague Dawley rat (B) 10 min after [^{18}F]**4** injection. Images from both striatal (left) and cerebellar (right) planes are presented.

We measured an IC_{50} value of PIB for Aβ plaques in vitro using [^{18}F]**4**. We have no data for the actual binding site for curcumin or PIB on Aβ in the APP23 mouse. In Supplementary data, table 1 is presented various determinations of K_d and K_i for curcumin, curcumin derivates and Aβ dye derivates. As can be seen, there is a very wide range for curcumin binding constant (K_D and K_i) against Aβ, ranging from 0.2 to 46,000 nM. This wide range can at least partly be explained by the different inhibitors used in the determinations or by methodological issues. In competition binding assays studies with curcumin and its ^{18}F-labelled derivates against the Thioflavine T derivate [^{125}I] IMPY or the Congo Red derivate [^{125}I] IMSB, the K_i values for curcumin and its derivates were in the low nanomolar range (see Supplementary data, table 1).[7,12,14] We chose to use PIB, a thioflavine derivate, as the inhibitor in the [^{18}F]**4** displacement studies. [^{11}C]PIB is by far the best characterized PET-tracer for imaging of Aβ. Based on earlier published data [34] we conclude that [^{18}F]**4** and PIB share the same high affinity binding site, since Congo Red and curcumine share the same high affinity binding site as do Congo Red and Thioflavine T. However, at least Congo Red and Thioflavine T have other low affinity binding sites as well as one other high affinity site for Thioflavine.[34] The IC_{50} of 100 μM of PIB determined for fibrilar Aβ using [^{18}F]**4** suggest that the binding site of [^{18}F]**4** is not strictly associated with the high-affinity binding site of PIB, although matching binding of [^{18}F]**4** and Thioflavin S in the APP23 tissue sections indicated otherwise.

With regard to the curcumin-like moiety of [^{18}F]**4**, the structure matches the properties shown to be important for BBB penetration and Aβ plaque binding. [^{18}F]**4** has two phenyl rings at appropriate distance and an enol-type arrangement due to the pyrazole moiety that creates coplanarity and extended double-bond conjugation through the center of the molecule; a structure shown to be important for Aβ plaque binding of curcumin derivates and should also facilitate the BBB penetration.[17–19,31] A similar pyrazole derivate of curcumin is the drug candidate CNB-001 that has been shown to penetrate BBB and to bind Aβ.[15] The co-planarity created by the pyrazole moiety creates a unique structure of [^{18}F]**4** that differs from earlier curcumin derivates developed as PET tracers.[7,10,12]

However, in addition to the curcumin-like structure [^{18}F]**4** has the {1-[2-(2-fluoroethoxy)ethoxy)ethyl)-1*H*-1,2,3-triazol-4-yl]methyl}acetamide group attached to the pyrazole ring. In CBN-001 there is a phenyl group attached to the pyrazole ring [15] and in the fluorinated curcumin analogs a fluoropegylated tail is attached to the aromatic structure.[7,14] These compounds all show ready passage through the BBB. In [^{18}F]**4** the acetamide group is in the centre of the molecule and the fluoropegylated tail is attached to the azide ring; the presence of this rather large non-aromatic group may cause hindrance in the BBB passage of the molecule. Also the molecular weight (635 Da) of [^{18}F]**4** is in the range where BBB passage is limited due to the high molecular weight.[32,33] Compounds that have molecular weight more than 400 Da but less than 657 Da have shown to have restricted ability to cross the BBB.[32,33] The overall large size and high molecular weight of [^{18}F]**4** are possible reasons for poor brain uptake.

Evaluation of [^{18}F]**4** ex vivo and in vivo revealed low brain uptake of the compound; this uptake was lower than that previously described for other ^{18}F-labeled curcumin derivates.[7,12] However, the healthy animals used for ex vivo autoradiography lack Aβ plaques and thus have no binding sites for [^{18}F]**4** in the brain. To further investigate brain uptake, in vivo studies were conducted with old transgenic animals with abundant Aβ deposition in the brain. Due to the high-affinity binding of [^{18}F]**4** to the Aβ plaques in this model that was observed in vitro, increased retention of [^{18}F]**4** in the APP23 brain was expected if the tracer crosses the BBB. However, no differences in brain uptake and retention were detected between APP23 and WT mice.

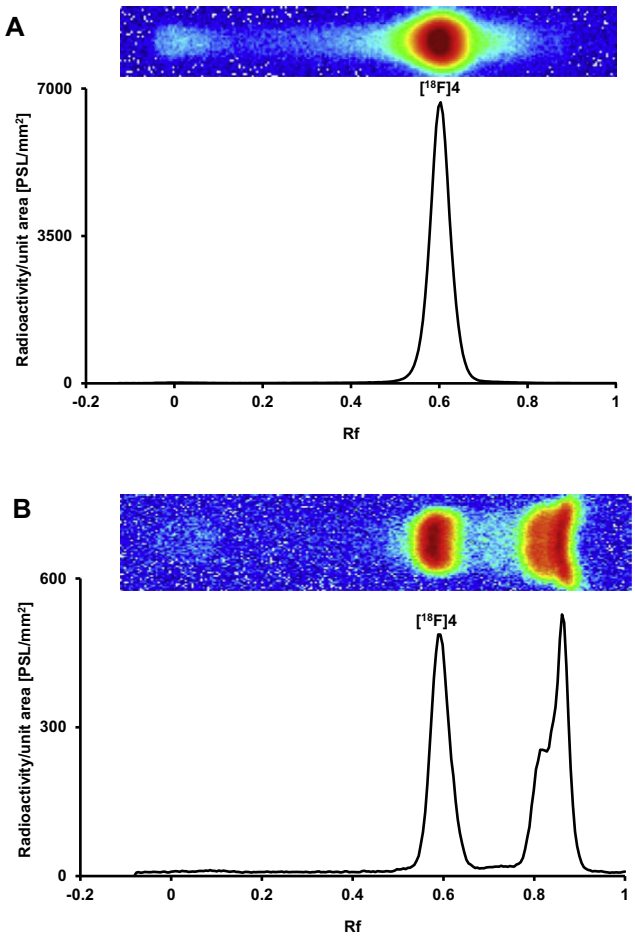

Figure 8. TLC analysis of radiometabolites of [^{18}F]**4** from rat plasma using autoradiography. Unchanged [^{18}F]**4** was used as reference standard. (A) Radiometabolic profile of [^{18}F]**4** from Sprague Dawley rat plasma 10 min after [^{18}F]**4** injection. (B) Plates were HPTLC Silica gel 60 RP-18W developed with a mixture of 1% acetic acid/methanol (2:8, v/v).

In previous studies, where low uptake in the brain was seen, it was suggested to be caused by rapid metabolism of the tracers in the liver, similar to that of curcumin.[6,12] In this study, unchanged [^{18}F]**4** still comprised 45% of the total ^{18}F-radioactivity in rat plasma 10 min post injection; rapid metabolism is therefore not expected to explain the low uptake in the brain. [^{18}F]**4** exhibited fast clearance from the blood to the liver, and fast hepatobiliary excretion to the intestine, where ^{18}F-radioactivity accumulated at a later phase. Similar excretion via the hepatobiliary system was previously observed with curcumin,[6] ^{18}F-fluoropegylated curcumin derivates [7] and ^{18}F-labeled fluoropropyl-substituted curcumin.[12] This indicates that [^{18}F]**4** metabolizes using hexahydrocurcumin-glucuroniside conjugate route,[6] although the metabolites of [^{18}F]**4** were not identified. The number of animals used for this study was low, but as low brain uptake was observed, further ex vivo experiments in animals were not considered necessary to the current investigation.

Although [^{18}F]**4** as such is probably not a workable PET-tracer, this study shows that further development of analogues of curcumin is a promising route for in vivo imaging of Aβ load. As non-toxic compounds, with strong Aβ binding as well as inhibition capacity towards both plaques as well as oligomers, curcumin analogs may have potential as tracers for early onset AD. Thus we plan to modify the structure of the curcumin analogue and to combine functionalized nanoliposomes with ^{18}F-labelled curcumin derivates in order to increase affinity and enhance transport through the BBB.

5. Conclusions

The [^{18}F]curcumin derivate [^{18}F]**4** was successfully synthesized with good radiochemical yield in a one-pot synthesis using nucleophilic ^{18}F-fluorination and click chemistry. In vitro studies of [^{18}F]**4** showed specific binding to Aβ in post mortem transgenic mouse brain; Aβ is considered a hallmark of AD pathology. However, [^{18}F]**4** has low in vivo BBB penetration and thus future studies are needed to reveal the reason for this and to possibly overcome this issue.

Acknowledgements

This study received funding from the European Community's Seventh Framework Programme (FP7/2007-2013) under Grant agreement no. 212043 and from the Academy of Finland Grant agreement 266891. The APP23 mice were used with the kind permission of Novartis Pharma, Swizerland.

Supplementary data

Supplementary data associated with this article can be found, in the online version, at http://dx.doi.org/10.1016/j.bmc.2014.03.010.

References and notes

1. Goel, A.; Kunnumakkara, A.; Aggarwal, B. *Biochem. Pharmacol.* **2008**, *75*, 787.
2. Hatcher, H.; Planalp, R.; Cho, J.; Torti, F.; Torti, S. *Cell. Mol. Life Sci.* **2008**, *65*, 1631.
3. Yang, F.; Lim, G.; Begum, A.; Ubenda, O.; Simmons, M.; Ambegaokar, S.; Chen, P.; Kayed, R.; Glabe, C.; Frautschy, S.; Cole, G. *J. Biol. Chem.* **2005**, *7*, 5892.
4. Begum, A.; Jones, M.; Lim, G.; Morihara, T.; Kim, P.; Heath, D.; Rock, C.; Pruitt, M.; Yang, F.; Hudspeth, B.; Hu, S.; Faull, K.; Teter, B.; Cole, G.; Frautschy, S. J. *Pharmacol. Exp. Ther.* **2008**, *326*, 196.
5. Lim, G.; Chu, T.; Yang, F.; Beech, W.; Frautschy, A.; Cole, G. *J. Neurosci.* **2001**, *21*, 8370.
6. Pan, M.-H.; Huang, T.-M.; Lin, J.-K. *Drug Metab. Dispos.* **1999**, *1*, 486.
7. Ryu, E.; Choe, Y.; Lee, K.-H.; Choi, Y.; Kim, B.-T. *J. Med. Chem.* **2006**, *49*, 6111.
8. Patel, P.; Collins, D.; Nistor, M.; Easwaramoorthy, B.; Head, E.; Mukherjee, J. *J. Nucl. Med.* **2007**, *48*, 22P.
9. Ran, C.; Xu, X.; Raymond, S.; Ferrara, B.; Neal, K.; Bacskai, B.; Medarova, Z.; Moore, A. *J. Am. Chem. Soc.* **2009**, *131*, 15257.
10. Al Jamaz, A.; Al-Otaibi, B.; Aboussekhra, A. *Q. J. Nucl. Med. Mol. Imaging* **2010**, *54*, 17.
11. Mourtas, S.; Canovi, M.; Zona, C.; Aurilia, D.; Niarakis, A.; La Ferla, B.; Salmona, M.; Nicotra, F.; Gobbi, M.; Antimisiaris, S. *Biomaterials* **2011**, *32*, 1635.
12. Cui, M.; Ono, M.; Kimura, H.; Liu, B.; Saji, H. *J. Med. Chem.* **2011**, *54*, 2225.
13. Yangisawa, D.; Amatsubo, T.; Morikawa, S.; Taguchi, H.; Urushitani, M.; Shirai, N. *Neuroscience* **2011**, *184*, 120.
14. Lee, I.; Yang, J.; Lee, J.-H.; Choe, Y.-S. *Bioorg. Med. Chem. Lett.* **2011**, *21*, 5765.
15. Liu, Y.; Dargusch, R.; Maher, P.; Schubert, D. *J. Neurochem.* **2008**, *105*, 1336.
16. Narlawar, R.; Pichardt, M.; Leuchtenberger, S.; Baumann, K.; Krause, S.; Dyrks, T.; Weggen, S.; Mandelkow, E.; Schmidt, B. *ChemMedChem* **2008**, *3*, 165.
17. Yanagisawa, D.; Shirai, N.; Amatsubo, T.; Taguchi, H.; Hirao, K.; Urushitani, M.; Morikawa, S.; Inubushi, T.; Kato, M.; Kato, F.; Morino, K.; Kimura, H.; Nakano, I.; Yoshida, C.; Okada, T.; Sano, M.; Wada, Y.; Wada, K.; Yamamoto, A.; Tooyama, I. *Biomaterials* **2010**, *21*, 4179.
18. Balasubramanian, K. *J. Agric. Food Chem.* **2006**, *54*, 3512.
19. Reinke, A.; Gestwicki, J. *Chem. Biol. Drug Des.* **2007**, *70*, 6944.
20. Nordberg, A.; Rinne, J.; Kadir, A.; Långström, B. *Nat. Rev. Neurol.* **2010**, *6*, 78.
21. Mathis, C.; Wang, Y.; Holt, D.; Huang, G.-F.; Depnath, M.; Klunk, W. *J. Med. Chem.* **2003**, *46*, 2740.
22. Klunk, W.; Engler, H.; Nordberg, A.; Wang, Y.; Blomqvist, B.; Holt, D.; Bergström, M.; Savitcheva, I.; Huang, G.; Estrada, S.; Ausén, B.; Debnath, M.; Barletta, J.; Price, J.; Sandell, J.; Lopresti, B.; Wall, A.; Koivisto, P.; Antoni, G.; Mathis, C.; Långström, B. *Ann. Neurol.* **2004**, *55*, 306.
23. Eckroat, T.; Mayhoub, A.; Garneau-Tsodikova, S. Beilstein. *J. Org. Chem.* **2013**, *1012*, 9.
24. Svedberg, M.; Rahman, O.; Hall, H. *Nucl. Med. Biol.* **2012**, *39*, 484.
25. Snellman, A.; Rokka, J.; Lopez-Picon, F.; Eskola, O.; Wilson, I.; Farrar, G.; Scheinin, M.; Solin, O.; Rinne, J.; Haaparanta-Solin, M. *Eur. J. Nucl. Med. Mol. Imaging* **2012**, *39*, 1784.
26. Cselényi, Z.; Jönhagen, M.; Forsberg, A.; Halldin, C.; Julin, P.; Schou, M.; Johnström, P.; Varnäs, K.; Svensson, S.; Farde, L. *J. Nucl. Med.* **2012**, *53*, 415.

27. Zhang, W.; Oya, S.; Kung, M.-P.; Hou, C.; Maier, D.; Kung, H. *Nucl. Med. Biol.* **2005**, *32*, 799.
28. Choi, S.; Golding, G.; Zhuang, Z.; Zhang, W.; Lim, N.; Hefti, F.; Benedum, T.; Kilbourn, M.; Skovronsky, D.; Kung, H. *J. Nucl. Med.* **1887**, *2009*, 50.
29. Sturchler-Pierrat, C.; Abramowski, D.; Duke, M.; Wiederhold, K.; Mistl, C.; Rothacher, S.; Ledermann, B.; Bürki, K.; Frey, P.; Paganetti, P.; Waridel, C.; Calhoun, M.; Jucker, M.; Probst, A.; Staufenbiel, M.; Sommer, B. *Proc. Natl. Acad. Sci. U.S.A.* **1997**, *94*, 13287.
30. Wang, Y.-J.; Pan, M.-H.; Cheng, A.-L.; Lin, L.-I.; Ho, Y.-S.; Hsieh, C.-Y.; Lin, J.-K. *J. Pharm. Biomed. Anal.* **1867**, *1997*, 15.
31. Airoldi, C.; Zona, C.; Sironi, E.; Colombo, L.; Messa, M.; Aurilia, D.; Gregori, M.; Masserini, M.; Salmona, M.; Nicotra, F.; La Ferla, B. *J. Biotechnol.* **2011**, *156*, 317.
32. Levin, V. *J. Med. Chem.* **1980**, *23*, 682.
33. Partridge, W. M. *J. Cereb. Blood Flow Metab.* **1959**, *2012*, 32.
34. Reinke, A.; Gestwicki, J. *Chem. Biol. Drug Des.* **2011**, *77*, 399.